SAND2015-9335J

Dynamic Recrystallization Model for Whisker and Hillock Growth

P.T. Vianco and M.K. Neilsen

Sandia National Laboratories

Albuquerque, NM

Introduction – Tin (Sn) Whiskers and Dynamic Recrystallization (DRX)

Tin (Sn) whiskers are not a recent development. Studies in the late 1930's investigated thin filaments that grew spontaneously from Sn coatings used for the corrosion protection of electronic hardware. It was soon recognized that these Sn filaments, or *whiskers*, could create short circuits in the same electronic equipment. Figure 1a illustrates whisker growth in the hole of a printed circuit board having an immersion Sn surface finish. The engineering solution was to contaminate the Sn with > 3 wt.% of lead (Pb). The result was that whisker growth was replaced with hillock formation (Fig. 1b) that posed a minimal reliability concern to electrical circuits. Today, Pb-containing finishes are being replaced with pure Sn coatings to meet environmental restrictions on Pb use. The same short-circuit concerns have been raised, once again, with respect to Sn whiskers.

The present authors have taken the approach that, in order to develop more widely applicable, first-principles strategies to mitigate Sn whisker formation, it is necessary to understand the fundamental mechanism(s) and rate kinetics underlying their development. Numerous mechanisms have been proposed by other authors to describe whisker growth, including static recrystallization by Boguslavsky and Bush [1].

However, the latter mechanism, as well as other proposed concepts, could not corroborate all of the mechanical or physical metallurgy behaviors that have been observed for whisker growth [2]. For example, whiskers can occur in multiple, elemental metals that include Cd, In, Zn, and Au [3 – 6]. Long whiskers have also been observed to grow from 52In-48Sn solder joints (Fig. 2a) and from Sn-Pb solder in metallographic mounts (Fig. 2b). In the latter case, Pb-whiskers grew out to the Pb-rich phase of Sn-Pb solder. Each of these different behaviors place less emphasis on crystallography- or dislocation-specific micro-mechanisms and instead, signify the activity of a more generalized mechanism.

The present authors have proposed that *dynamic recrystallization (DRX)*, together with long-range diffusion, are the underlying mechanisms responsible for the growth process of whiskers [7 – 9]. Literature data as well as experiments described in references 7 – 9 have led the authors to conclude that DRX is the rate controlling mechanism for Sn whisker development. There appears to be few microstructural features that hinder the long-range diffusion of atoms in coatings having thicknesses of engineering relevance. The only limitation is thermal activation under environmental temperatures. In the case of Sn, even room temperature represents a high homologous temperature – the ratio of existing temperature (e.g., 298K) to the solidus temperature (505K), or 0.59 – that allows for the ready self-diffusion Sn atoms in the film. A similar condition prevails for whisker formation in other metals and alloys.

Development of the DRX model was based upon the following stipulations. First of all, whiskers of greatest concern to electronics reliability are defined as *long whiskers* (Fig. 3a). A geometric definition for long whiskers describes those filaments that have a

length-to-width ratio that exceeds five (5) [9]. The functional definition of long whiskers is that they are created by *cyclic DRX*. As the term implies, cyclic DRX occurs when there are multiple cycles of new grain initiation followed by grain growth. The driving force for multiple DRX cycles is required at the initiation site in order to develop long-length whiskers. The second variant is *continuous DRX*. Continuous DRX typically has one or at most, two such recrystallization cycles and is responsible for short, stubby whiskers (e.g., Fig. 3b).

The schematic diagram in Fig. 4 illustrates the manner whereby DRX creates a long whisker. (a) Strain energy is created in film as represented by the dislocations. (b) The first DRX cycle begins with initiation of a new grain. Note that the grain boundary is pinned in place. (c) The new grain grows until it consumes the old grain, thereby completing the first DRX cycle. (d) A significant amount of strain energy remains in the thin film "system." Under relatively easy, long-range diffusion, it is more advantageous for the system to release strain energy by continuing the DRX grain growth at the established site. (e) Because the left-hand side boundary is pinned, the new grain growth continues out of the surface. In effect, the extension of the whisker by each unit of grain size represents a DRX cycle. If the strain energy is initially limited, the added grain growth stop at the stage shown in Fig. 4d, resulting in a short, stubby whisker.

The ease of Sn diffusion allows the thin film to act as a single "system" having a total strain energy. The length and number of long whiskers are determined by the number of grains that participate in the DRX process. A few such grains will grow only a few whiskers. But, those whiskers will grow long. And, visa-versa is true.

Boettinger, et al. concluded that long whiskers and hillocks are generated by the same mechanism (which they proposed to be an "extrusion-like" plastic flow process rather than the DRX mechanism) [10]. The factor that distinguishes between whisker and hillock growth is grain boundary pinning. As shown in Fig. 4, long whiskers require pinning of the initial grain boundaries. When grain boundary pinning is absent, hillocks form because lateral grain growth can take place. Hillock growth is illustrated by the schematic diagram in Fig. 5. As noted in Fig. 5a, the initiation of DRX is the same as that that leads to long whisker growth. However, in Fig. 5b, there is the absence of grain boundary pinning. The greater contribution of lateral growth results in the customary hillock shape as shown in Fig. 5c.

The schematic diagrams in Figs. 4 and 5, as well as several variants that are discussed in reference 9, provide qualitative illustrations of the means whereby DRX, in conjunction with long-range diffusion, can generate the whisker and hillock structures that are observed in thin films. Next, a quantitative model is constructed to predict DRX under the deformation, temperature, and time parameters that are commensurate with conditions responsible for whisker development. Tin was selected for this analysis in order to apply the study results to engineering applications.

The first step towards developing a quantitative model was to identify a criterion for DRX initiation. That criterion is the critical strain, ε_c. The critical strain represents the lower limit of anelastic strain (energy) required to initiate DRX (Fig. 4a). The critical strain is calculated by the following equation [11, 12]:

$$\varepsilon_c = A\, D_o^m\, Z^n, \qquad (1)$$

In equation (1), A, m, and n are material constants. The initial grain size is represented by D_o and Z is the Zener-Hollomon parameter, which is expressed as:

$$Z = d\varepsilon/dt(\exp\Delta H/RT), \qquad (2)$$

where $d\varepsilon/dt$ is the strain rate (which includes the stress, σ, implicitly); ΔH is the apparent activation energy; R is the universal gas constant; and T is temperature. The value of ΔH is calculated from the steady-state or minimum creep rate at stress and temperature because the creep strain (energy) creates the driving force for DRX and, as such, controls whisker or hillock growth.

The second step was to develop the means to predict the anelastic strain, ε, in the films as a function of temperature and stress. The value of is ε is compared against ε_c so that, when the criterion, $\varepsilon > \varepsilon_c$, is met, there can be the initiation of DRX. A computational model was developed to predict ε. The available material properties database of 100Sn was not sufficiently complete to provide the parameters needed to construct a unified creep-plasticity (UCP) constitutive equation that is essential to such a model. Therefore, the decision was made to use the UCP constitutive equation for 95.5Sn-3.9Ag-0.6Cu (wt.%) solder as a surrogate for 100Sn [13]. The analysis that is described in reference 9 supported the use of this approximation.

The third step was to develop a set of experiments that allowed for observing long whiskers and hillocks as a function of temperature and strain conditions. An important goal was to remove “uncontrolled” contributors to the anelastic strain from the test

specimens. Those contributors include electroplating additives, intermetallic compound (IMC) layer growth, excessive internal stresses, and variable microstructures. Therefore, the test sample configuration was chosen as physical vapor deposited Sn layers on 25.4 mm diameter, silicon (Si) substrates. The evaporation process created repeatable, columnar microstructure across all Sn film thicknesses.

The fourth, and final, step was to validate the DRX model by combining together the critical strain (ε_c) calculated by equation (1), strain predictions (ε) made by the constitutive model, and empirical, whisker and hillock data. More specifically, validation required that the appearance of long-whiskers and hillocks (i.e., cyclic DRX) correlate with the criterion of $\varepsilon > \varepsilon_c$. This step also took into account the *thin film effects* of the Sn coating because they impact the grain growth phase of DRX. The thin film effects turn out to be a significant factor for completing the picture of observed long whisker and hillock development based on the DRX model.

The discussions are provided in the following four sections that describe the analyses used to complete the four steps:

- Creep Deformation Analysis Establishes the Critical Strain (ε_c),
- Computational Model is Used to Predict Anelastic Strain (ε),
- Empirical Data: Long Whiskers and Hillocks Versus Temperature and Thickness, and
- Validation of the DRX Mechanism.

Creep Deformation Analysis Establishes the Critical Strain (ε_c)

The creep experiments were carried out on samples that were hollow cylinders of 100Sn. The cylinders were cast, and then machined to final shape, in order to create a pseudo-columnar grain orientation perpendicular to the applied load. This geometry represented a scaled-up version of the microstructure-applied stress relationship observed in thin films. The sample configuration is shown in Fig. 6. The left-hand image is a schematic diagram of the hollow cylinder. The center micrograph shows the pseudo-columnar microstructure of the cylinder wall. The sample is placed in the test frame as shown by the right-hand photograph. Creep tests were performed under constant load control. Duplicate tests were performed under these temperatures: 0°C, 25°C, 50°C, 75°C, and 100°C as well as these stresses: 1 MPa, 2 MPa, 5 MPa, and 10 MPa. All of these conditions are commensurate with those predicted in Sn coatings that exhibit whisker and hillock growth.

The creep experiments provided the following information. First, the apparent activation energy, ΔH, was calculated from the steady-state creep rate. Two creep regimes were delineated by strain rates above, and below, $10^{-7}\ s^{-1}$. Those regimes were identified by different ΔH values:

(a) "Slow" strain rate ($< 10^{-7}\ s^{-1}$), $\Delta H = 8 \pm 9$ kJ/mol, and

(b) "Fast" strain rate ($> 10^{-7}\ s^{-1}$), $\Delta H = 65 \pm 6$ kJ/mol.

The presence of two deformation regimes affects ε_c as calculated by equation (1) through the Z parameter. Values of A, m, and n were obtained for equation (1), using data in reference 14. The value of D_o was 350 μm (Fig. 6). The graph is shown in Fig. 7 of strain as a function of nominal (creep) stress and test temperature. The closed symbols are the ε_c values predicted by equation (1). There is nearly four orders of magnitude

difference in ε_c between the two ΔH regimes. This trend indicates that the DRX mechanism, and the resulting whisker and hillock development activities, are very sensitive to the strain rate experienced by the Sn film under the loading conditions.

Secondly, the open symbols in Fig. 7 indicate the ε_{max} values that were reached in those experiments. The ε_{max} values fell between the two critical strain regimes, which confirms that the experiments were testing within the deformation "space" of whisker growth in Sn films. At stresses less than approximately 5 MPa, this condition persists $\varepsilon_{max} > \varepsilon_c$, which implies that DRX should take place. Evidence to this effect was observed in the samples. However, the grain size was too large to support actual whisker or hillock development. At stresses greater than 5 MPa, the $\varepsilon_{max} < \varepsilon_c$ and DRX would not be predicted in those samples. It is important to reiterate that, although stress is the independent variable in Fig. 7, in fact, it is the strain rate through Z in equation (2) that controls the relationship between ε (ε_{max} in Fig. 7) and ε_c.

Computational Model is Used to Predict Anelastic Strain (ε)

Development of the computational model began with building the finite element representation for the Sn film/Si wafer test specimen. The finite element construct, which was reduced to a one-quarter slice, is shown in Fig. 8. The wafer is supported around its outer circumference approximately 1 mm inboard from the edge. The zero load condition is shown at the top and the 500g load that places the Sn film in *tension* is shown in the bottom diagram. The minimum and maximum displacements are also shown in the latter picture. The strain gradient is negligible in the through-thickness dimension of all films. A second contribution of anelastic strains was generated by the

mismatch between the coefficients of thermal expansion (CTE) between Si (2.6 ppm/°C) and Sn (22 ppm/°C). Unlike the "500g loading" strains, the CTE mismatch strains are distributed uniformly across the wafer and similarly do not generate a strain gradient through the thickness of the Sn.

The computational model calculated the anelastic strains in the radial, hoop, and thickness directions. Because the strain (energy) is a scalar quantity that controls DRX, it was not necessary to understand the details of the strain vector. Rather, the appropriate output from the model was the von Mises strain, which was termed the *equivalent plastic strain* (EQPS).

An important feature of the computational model was that it predicted both EQPS and strain rate as a function of time at temperature. Thus, the EQPS could be partitioned between that accumulated at a strain rate greater than 10^{-7} s^{-1} and the strain contribution at strain rates less than 10^{-7} s^{-1}. As will be shown later, this step is critical to the model validation.

Empirical Data: Long Whiskers and Hillocks Versus Temperature and Thickness

The test samples were constructed of Si wafers measuring 25.4 mm in diameter and 0.275 mm in thickness. Thin films were applied by physical vapor deposition (PVD) using the evaporation technique to eliminate ancillary factors that would affect whisker and hillock growth, thereby complicating the data analysis. The polished wafer surface was first coated with a 20 nm thick chromium (Cr) adhesion layer. The Sn film was then evaporated onto the Cr surface without a break in the vacuum. The Sn film thicknesses

were 0.25, 0.50, 1.0, 2.0, and 4.9 μm. Focused ion-beam (FIB) cross sections confirmed that adhesion was maintained at all interfaces.

The test environments were as follows: Annealing temperatures were 35°C, 60°C, 100°C, 120°C, and 150°C. The heating rate was 15°C/min. All annealing treatments were performed in air. A single time period was used – nine (9) days – because previous research indicated that whisker and hillock growth was largely completed in these samples within seven days [9].

As briefly noted above, two methods were used to introduce strain (energy) into the films. The first technique used the CTE mismatch between Sn and Si to generate strains within the order of 10^{-3}. The second method applied a 500 g load to the center of the wafer, resulting in strains within the order of 10^{-4}. In the latter case, there were three conditions: compression, tension, and zero load. Applying strains that encompass two orders of magnitude provided a means to investigate the sensitivity of the DRX mechanism to the level of strain energy in the films.

The film surfaces were examined for either the *presence* or *absence* of long-whiskers and hillocks. It was not necessary to provide a precise, quantitative assessment of each phenomenon (e.g., lengths and number of whiskers) in order to validate the DRX model. The 500 g load condition was also recorded as: compression, "C;" tension, "T;" and zero "N."

Validation of the DRX Mechanism

The Sn film/Si wafer test specimens were evaluated for long whiskers and hillocks. Images exemplify these two phenomena in Figs. 9a and 9b, respectively. The

data analysis determined that the 500g load, whether it placed the film into tension or compression, or was absent altogether, did not affect the presence of either phenomenon. Therefore, the DRX mechanism was not affected by the strain energy created by EQPS values within, or less than, the order of magnitude of 10^{-3}.

The premise was stated that both long whiskers and hillocks are consequences of the same DRX mechanism and, more specifically to the present study, cyclic DRX. Therefore, the long whisker and hillock data sets were combined together into a single table, Table 1. Thus, Table 1 indicates cyclic DRX as a function of test temperature and film thickness. (It was not necessary to include the presence of the 500g load – that effect was concluded earlier to be negligible.) The dashed white line establishes the boundary between the presence of cyclic DRX (green) and its absence (red). In general, Table 1 shows that there is a limited presence of cyclic DRX in the 0.25 μm films. There is a strong presence of it in the 0.5 μm and 1.0 μm films. Lastly, cyclic DRX diminished significantly in the 2.0 μm and 4.9 μm coatings. These trends, together with the more detailed data specific to each of the long-whisker and hillock phenomena, established the empirical database for the validation exercise.

The steps in the predictive capability began with calculating critical strain for the two ΔH regimes, using equation (1). Film thickness represented the initial grain size, D_o. Next, the computational model was used to predict EQPS and the corresponding strain rate, $d\varepsilon/dt$, in the films. Then, the predicted EQPS was partitioned by ΔH regime in order to compare those values against the respective ε_c values for each such regime. Those comparisons between EQPS and ε_c predicted the initiation of DRX. Lastly, those

predictions were compared to the empirical data in Table 1 as the final step to validate the DRX model.

The analysis begins by recalling that the strain rate of 10^{-7} s^{-1} distinguished the two ΔH regimes: 8 kJ/mol for $d\varepsilon/dt < 10^{-7}$ s^{-1} and 65 kJ/mol for $d\varepsilon/dt > 10^{-7}$ s^{-1}. Using equation (1), the values of ε_c were calculated as a function of temperature and film thickness for $d\varepsilon/dt = 10^{-7}$ s^{-1}. The results are plotted as strain versus temperature in Fig. 10. There are the "ΔH = 65 kJ/mol" critical strain curves (dashed lines) and the "ΔH = 8 kJ/mol" curves (solid lines). The symbols distinguish each curve according to film thicknesses. A strain rate that is faster than 10^{-7} s^{-1} would generate a new set of critical strain curves using 65 kJ/mol in equation (1). Those curves would be above the "ΔH = 65 kJ/mol" curves currently in Fig. 10. A strain rate less than 10^{-7} s^{-1} would create a new set of "8 kJ/mol" critical strain curves that would be below those in Fig. 10.

Next, the computational model was used to calculate the EQPS in the films, which was then partitioned between the two ΔH regimes. The assumption was made that the DRX behavior that occurs within the slow strain rate regime (8 kJ/mol) regime is independent of that that takes place before it at fast strain rates (65 kJ/mol). The premise was based upon the work of Gottstein [15]. The strain partitioning was performed for each test temperature. Since anelastic strain was not sensitive to film thickness; location within the film thickness; or the position on the wafer, the model was executed using these selected conditions: (a) 4.9 μm thickness; (b) top surface; (c) no load; and (d) the 4.0 mm position. The results are plotted as the two red lines in Fig. 10. The dashed line represents EQPS that accumulated under strain rates greater than 10^{-7} s^{-1}. At temperatures below 60°C, the arrow implies that the strain contribution drops to

effectively zero. The solid line represents strains that built up at strain rates less than 10^{-7} s^{-1}.

The analysis of Fig. 10 begins by considering temperatures less than 80°C. The dashed red line is well below the associated ε_c curves, indicating that $\varepsilon < \varepsilon_c$ and that the strain contribution at strain rates greater than 10^{-7} s^{-1} is insufficient to support DRX at any film thickness. On the other hand, the red solid line, which is the strain accumulated at strain rates less than 10^{-7} s^{-1}, is above the ε_c curves. Therefore, the $\varepsilon > \varepsilon_c$ criterion is satisfied and DRX is predicted to take place. In the latter case, the likelihood for DRX is greater in the thinnest films, which corresponds to the trends observed in Table 1 with the exception of the 0.25 μm film that was a special case that was elaborated upon in reference 9.

The 80 – 125°C temperature range is examined next. The EQPS experienced at strain rates greater than 10^{-7} s^{-1} increased significantly. Meeting the criterion of $\varepsilon > \varepsilon_c$ depended strongly upon film thickness. The thinner films (0.25 – 1.0 μm) met the criterion and would support DRX. The thicker films, 2.0 μm and 4.9 μm were less likely to experience DRX at this strain rate. At the slow strain rates, the criterion for $\varepsilon > \varepsilon_c$ was met for all films except the 4.9 μm samples. Under both conditions of fast and slow strain rate, the dashed and solid red lines, respectively, predict that the 2.0 μm films were "borderline" with respect to initiating DRX. Table 1 indicates an absence of cyclic DRX. However, these films generated a significant quantity of short stubby whiskers (Fig. 3b). Therefore, DRX did initiate in the 2.0 μm coatings; but, it only progressed through the one or two cycles that characterize *continuous* DRX.

The temperature range of 125°C to 150°C is predicted to support DRX for all of the films under one, or both, strain rate regimes. For example, in the case of the thinner films of 0.25 – 1.0 μm, the $\varepsilon > \varepsilon_c$ criterion was met under *both* strain rate regimes. On the other hand, long whiskers and hillocks were predicted to occur in the 2.0 μm and 4.9 μm films due largely to strains accumulated at strain rates greater than 10^{-7} s^{-1} and most likely so, at temperatures approaching 150°C. These predictions corroborated the data in Table 1.

As a brief summary, validation of the cyclic DRX model was obtained by a comparison between: (a) the experimental data in Table 1; (b) the critical strains calculated of equation (1); and (c) the EQPS-at-strain rate predictions made by the computational model. The points (b) and (c) culminated into Fig. 10. The presence of short, stubby whiskers in the 2.0 μm films (and their occasional observation in 4.9 μm films) indicated that continuous DRX could occur under the borderline conditions of meeting the critical strain criterion for DRX. Lastly, any differences between the constitutive behaviors of Sn-Ag-Cu versus 100Sn in the computational model would change only slightly the relative positions of the two red strain curves in Fig. 10.

Further refinement was made of the correlation between the occurrence of long whiskers or hillocks and predictions made by the DRX model. The primary criteria remains as equation (1), which describes the capacity for strain (energy) to exceed the critical strain (energy) required to initiate DRX. Once DRX can start in a grain, the next stipulation is that the DRX be cyclic to form long whiskers and hillocks. This condition is expressed by equation (3):

$$D_o < 2D_r \qquad (3)$$

where D_o is the initial grain size and D_r is the final, recrystallize grain size [16]. Equation (3) indicates that the final grain size must be at least twice the initial grain size to allow multiple cycles that define cyclic DRX. Sakai and Jonas observed that when D_o is equal to, or slightly exceeds $2D_r$, the DRX that initiates will be continuous, having one or two cycles, which the 2.0 μm thick films substantiated, as described above [16].

The criterion based on equation (3) is somewhat more difficult to apply to the development of long whiskers and hillocks because they grow by the addition of atoms supplied from distant grains. If the metric, D_r, is the maximum dimension of a long whisker or hillock, then it can have values of tens of microns, twice the value of which well-exceeds D_o. Therefore, if the value of D_r in equation (3) refers to the largest dimension observed for long whiskers and hillocks, then the criterion is met by D_o equaling all of the film thicknesses.

On the other hand, D_o can be considered to be the in-plane dimension of long whiskers and hillocks. In the case of hillocks, the definition of D_r is unchanged. However, D_r is only 1.0 – 1.5 μm in the case of long whiskers. Equation (3) indicates that cyclic DRX would take place only in those films having a nominal grain size (thickness) less than 2.0 – 3.0 μm. This scenario, which certainly presents a more restrictive condition, corroborates the preference for cyclic DRX in films of 1.0 μm or less per Table 1.

Regardless of the interpretation for D_r, equation (3) predicts hillock formation when conditions satisfy the $\varepsilon > \varepsilon_c$ criterion. Therefore, hillocks should always accompany long whiskers. In fact, the two phenomenon did *not* always occur simultaneously. Observations were: 0.25 μm, hillocks; 0.5 μm, long whiskers; and 1.0

μm, both long-whiskers and hillocks. Both phenomena dropped off at the thicker films because they could not meet the $\varepsilon > \varepsilon_c$ criterion except at T>125°C. Short stubby whiskers were observed in the 2.0 μm films at T<125°C, indicating that continuous DRX could take place when $\varepsilon > \varepsilon_c$ was met, but only marginally so.

There is a third and final condition that affects long whisker and hillock growth. That condition is based upon the relationship between film thickness, h and the initial, in-plane grain diameter, d. That relationship controls the prevalence of *grain boundary pinning*. When d > h, the boundaries tend to pin, which as explained earlier, promotes long whisker growth over hillock development. Conversely, when d < h, which is the case with columnar grains, grain boundary pinning is less likely to occur, encouraging lateral grain growth that forms hillocks. Referring to the current test cases, the 0.5 μm films had film dimensions that were either d > h or d ≈ h, which suggests a preference for grain boundary pinning. In fact, long whiskers were preferred in these films. The 1.0 μm films exhibit d ≈ h or d < h conditions, which favors the appearance of hillocks. Both long whiskers and hillocks were observed in these samples.

In summary, the DRX model was validated by comparing empirical data of long-whisker and hillock growth to predictions based upon the critical strain criterion and constitutive model predictions of strain and strain rate. A "fine tuning" of that validation required the incorporation two additional stipulations that addressed: (a) cyclic DRX versus continuous DRX, and (b) the prevalence for grain boundary pinning.

Conclusions

1. Dynamic recrystallization (DRX), together with long-range diffusion, are proposed as the first-principles mechanisms responsible for whisker and hillock growth in Sn films.
2. Empirical data were obtained from test specimens having evaporated Sn films on Si wafers. The presence or absence of long whiskers and hillocks were recorded from the samples. Long whiskers and hillocks data were combined together to establish the presence of cyclic DRX.
3. The critical strain was calculated for the two ΔH regimes.
4. A computational model was used to predict the anelastic strain and strain rates based on the constitutive behavior of 95.5Sn-3.9Ag-0.6Cu (wt.%) as a surrogate for Sn.
5. The validation was made by comparing the experimental observations of long whiskers and hillocks against the critical strain criterion together with model predictions of anelastic strain (EQPS) and strain rate.
6. Long-range diffusion was not a controlling mechanism except at the lowest temperature ($T<35°C$) due to reduced thermal activation.
7. This model can be extended to long-whisker and hillock growth in other metal and alloy systems, given an availability of the appropriate materials properties.

Acknowledgments:

The authors wish to thank Dr. Lisa Deibler for her thorough review of the manuscript. Sandia is a multiprogram laboratory operated by Sandia Corporation, a Lockheed Martin Company, for the United States Department of Energy's National Nuclear Security Administration under Contract No. DE-AC04-94AL85000.

References

[1] I. Boguslavsky and P. Bush, *Proc. APEX 2003,* (IPC, Northbrook, IL; 2003) S12-4-1.

[2] G. Gaylon, iNEMI Monograph (iNEMI, Herdon, VA; 2003).

[3] NASA Goddard Space Flight Center, Website "Other Metal Whiskers", http://nepp.nasa.gov/whisker/other_whisker/index_htm

[4] P. Key, *Proc. IEEE Electronic Components Conference* (IEEE, New York, NY; 1975) 155.

[5] J. Busse, "Whiskers of Tin-Lead (Sn-Pb) on Reflowed Die Attach Solder Used in the Manufacture of a Laser Diode Array," NASA Web Site (2003).

[6] U. Lindberg *Acta Metall.* **24** 181 (1976).

[7] P. Vianco and J. Rejent, *J. Elect. Materials* **38** 1815 (2009).

[8] P. Vianco and J. Rejent, *J. Elect. Materials* **38** 1826 (2009).

[9] P. Vianco, M. Neilsen, J. Rejent, and R. Grant, *J. Elect. Materials* (2015) DOI: 10.1007/s11664-015-3779-4.

[10] W. Boettinger, C. Johnson, L. Bendersky, K.-W. Moon, M. Williams, and G. Stafford, Acta Materialia, 53, 5033 (2005).

[11] M. Barnett, G. Kelly, and P. Hodgson, Scr. Mater. 43, 13 (2000).

[12] M. Barnett, G. Kelly, and P. Hodgson, Metall. Mater. Trans. A, 33A, 1893 (2002).

[13] M. Neilsen and P. Vianco, "UCPD Model for Pb-Free Solder," *J. Elect. Packaging* (2014) DOI:10.1115/1.4026851.

[14] F. Thijssen, "Effect of Strain on Microstructural Evolution During Dynamic Recrystallization: Experiments on Tin," PhD Thesis, Ultrecht University (2004).

[15] G. Gottstein, Metal Sci. 17, 497 (1983)

[16] T. Sakai and J. Jonas, Acta Metall. 32, 189 (1984)

Figures

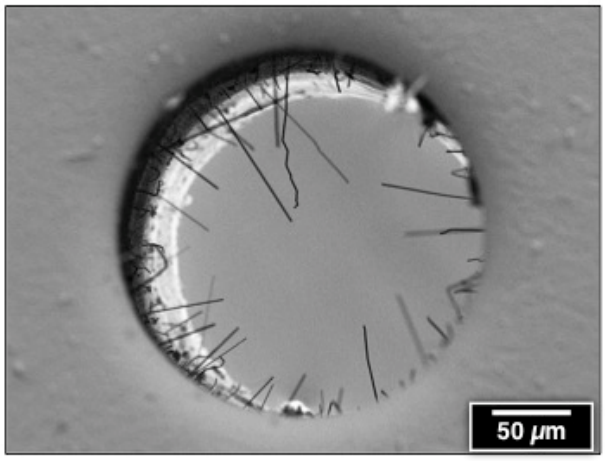

(a)

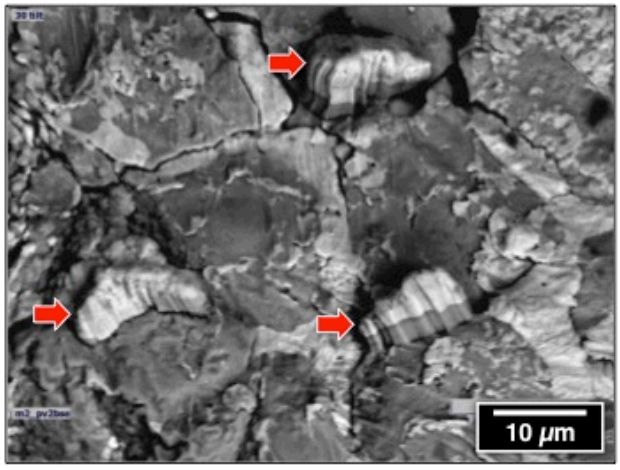

(b)

Fig. 1 (a) Tin whiskers formed within the hole of a printed circuit board having an immersion Sn finish. (b) Short, stubby whiskers grow from a 63Sn-37Pb (wt.%) coating on the lead of an electronic component.

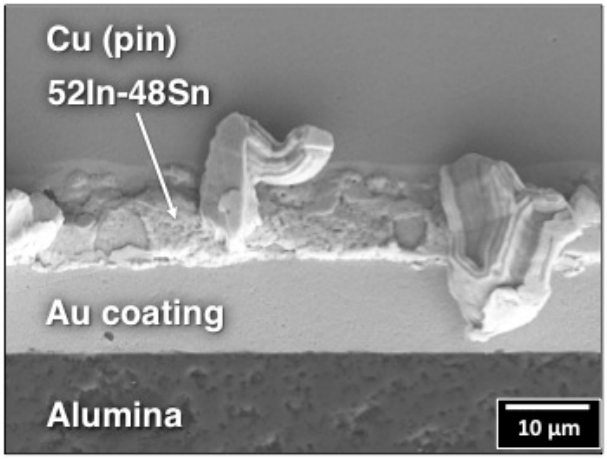

(a)

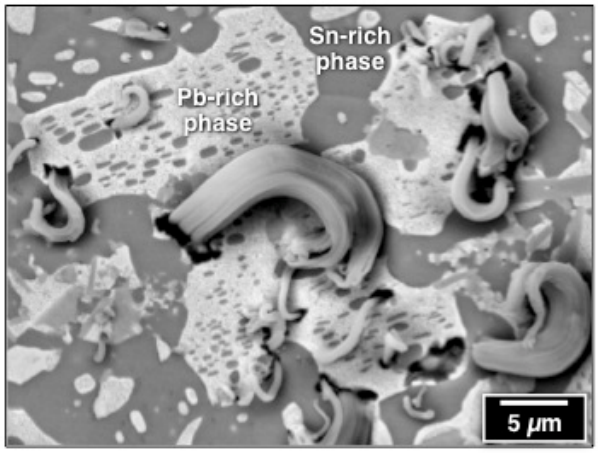

(b)

Fig. 2 (a) Whiskers grew from a 52In-48Sn (wt.%) solder joint that formed a joint between Cu and an alumina substrate. (b) Lead (Pb) whiskers developed from the Pb-rich phase of Sn-Pb solder after 2 days at 25°C.

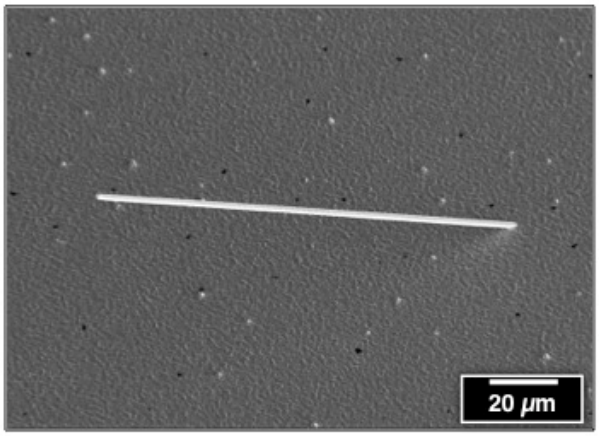

(a)

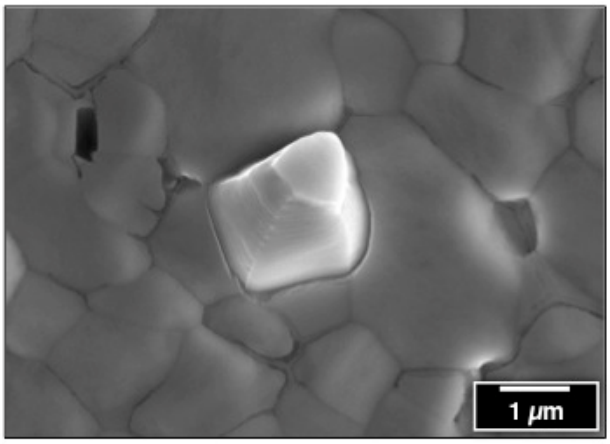

(b)

Fig. 3 (a) Long whisker grew from a 1.0 μm thick Sn film on a Si substrate and (b) a short, stubby whisker that developed from a 2.0 μm Sn film. Both samples were exposed to 100°C (air) for 9 days.

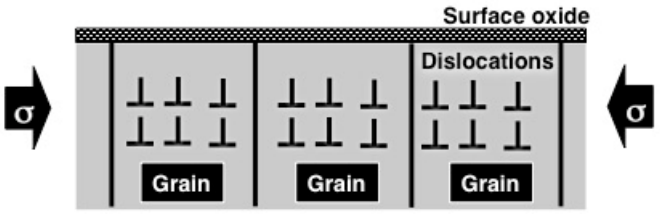
Surface oxide
Dislocations
σ
σ
Grain
Grain
Grain

(a)

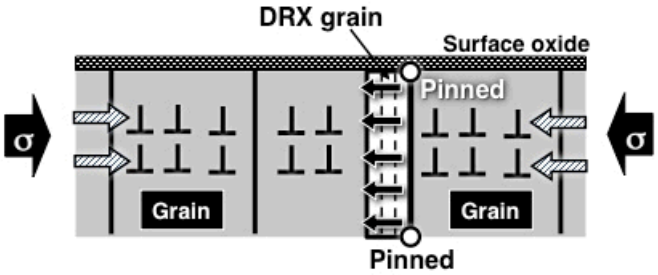
DRX grain
Surface oxide
Pinned
σ
σ
Grain
Grain
Pinned

(b)

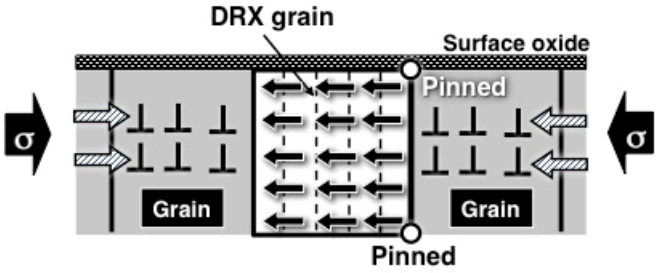
DRX grain
Surface oxide
Pinned
σ
σ
Grain
Grain
Pinned

(c)

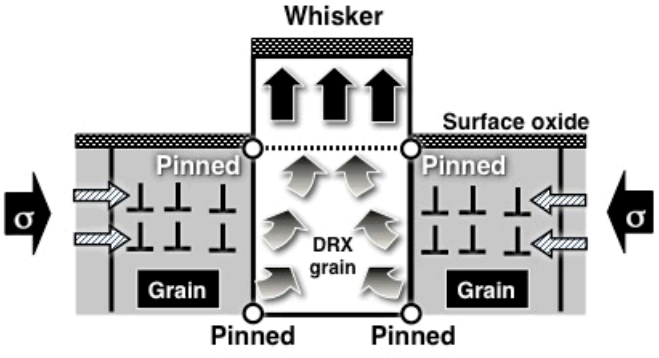
Whisker
Surface oxide
Pinned
Pinned
σ
σ
DRX
grain
Grain
Grain
Pinned
Pinned

(d)

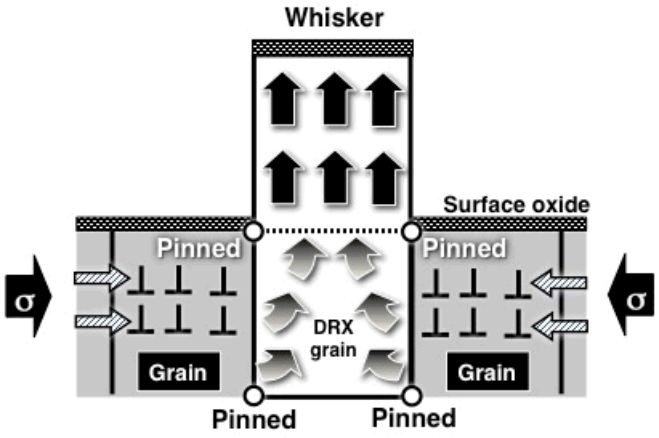

(e)

Fig. 4 Schematic diagram illustrates the growth of long whiskers by the DRX mechanism, and supported by long-range diffusion. (a) Strain energy (dislocations) provides the driving force. (b) Recrystallization initiates at the pre-existing grain boundary. (c) New grain growth consumes the initial grain. (d) Because both, initial boundaries are pinned, further lateral growth comes to a halt and the DRX process generates grain growth out of the surface. (e) The stain energy of the thin film "system" continues the grain growth process at this preferred site, generating the long whisker.

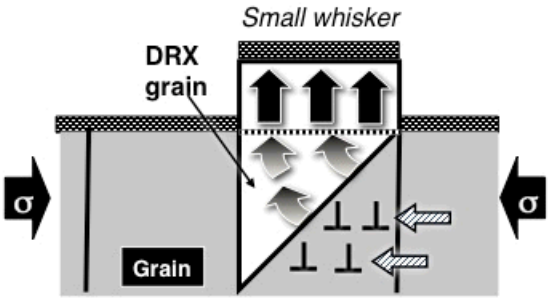

(a)

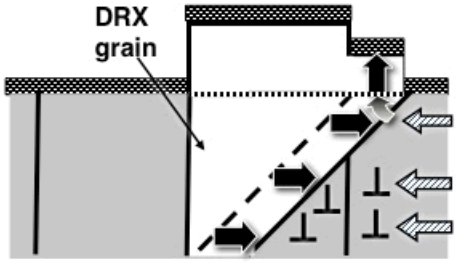

(b)

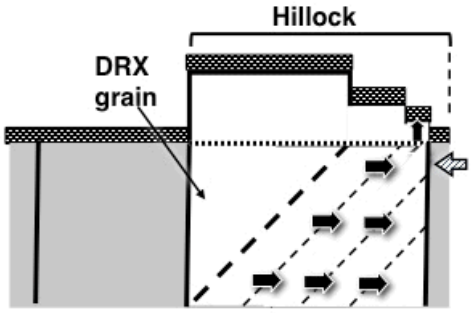

(c)

Fig. 5 Schematic diagrams illustrate hillock growth under the same DRX and long-range diffusion mechanisms. (a) The DRX process begins in the pre-existing grain and continues to the extent of even beginning a small whisker. (b) But, in the absence of grain boundary pinning, both vertical and lateral grain growth take place. (c) Lateral grain growth becomes the predominant component, giving rise to the hillock configuration.

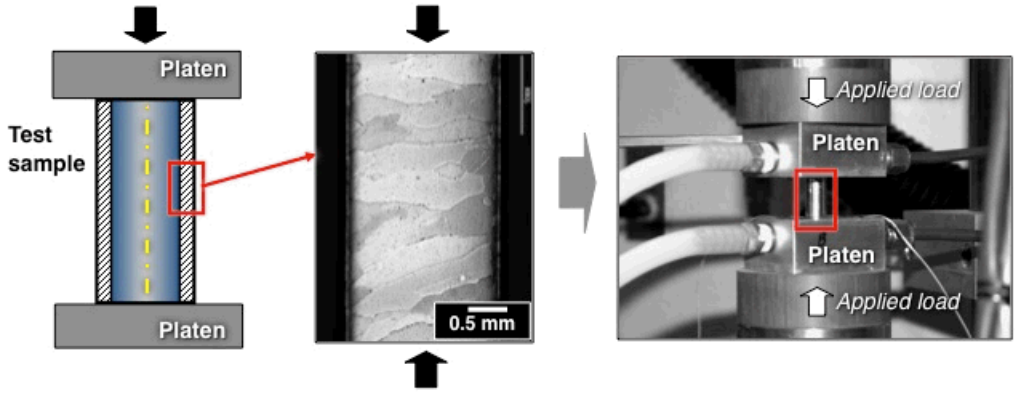

Fig. 6 Test configuration used to obtain the creep behavior of Sn from hollow cylindrical samples. The left-hand image is a schematic diagram of the cylinder. The micrograph in the center shows the pseudo-columnar grain structure generated in the cylinder wall. The right-hand photograph shows the sample in the test frame.

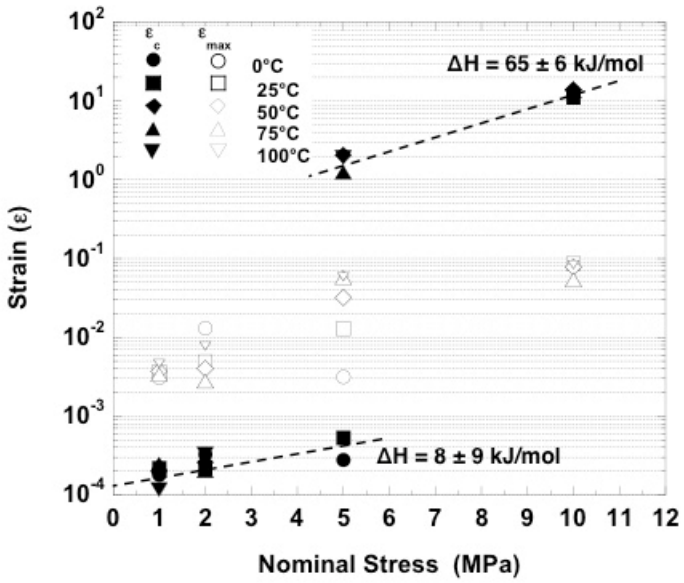

Fig. 7 Plot shows strain as a function of nominal stress and temperature. The solid symbols are the critical strains, ε_c, calculated by equation (1), using the two values of ΔH as noted on the graph. The open symbols are the maximum strains, ε_{max}, that were obtained from the hollow cylinder creep tests.

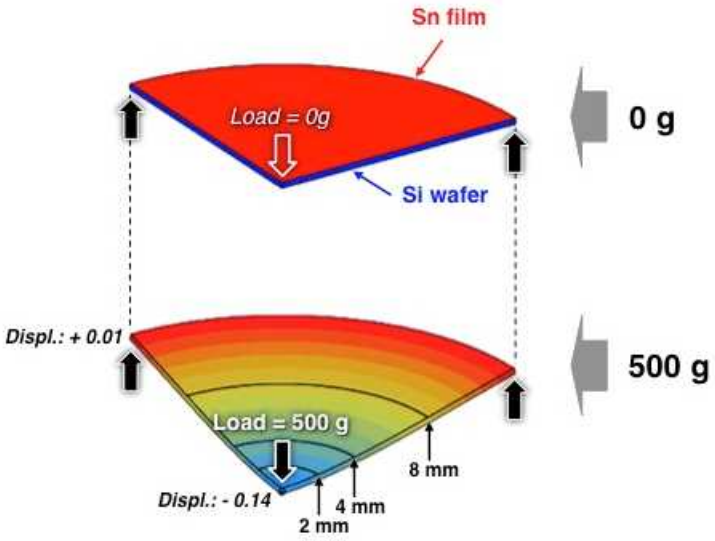

Fig. 8 Finite element constructs show the Sn film/Si wafer test specimen in the no-load condition (top) and the 500 g load condition (bottom) that placed the Sn film into *tension*. The minimum and maximum displacements are indicated in the picture.

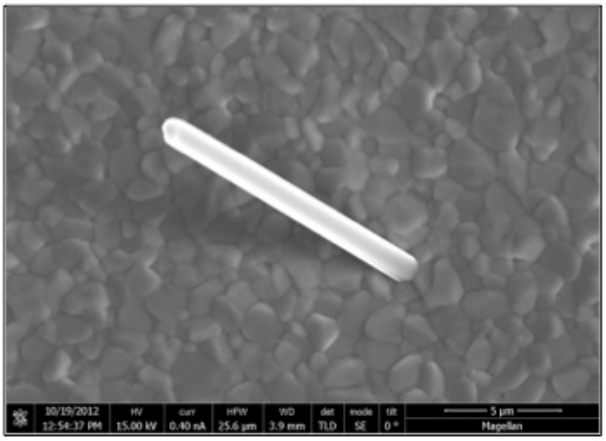

(a)

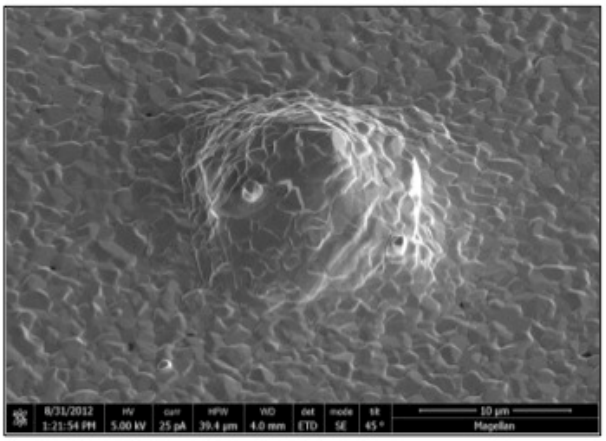

(b)

Fig. 9 (a) SEM image shows a long whisker that developed from a 1.0 µm film held for nine days at 60°C under no load. (b) Hillock formed on a 1.0 µm film exposed to 100°C for nine days under 500 g, compression.

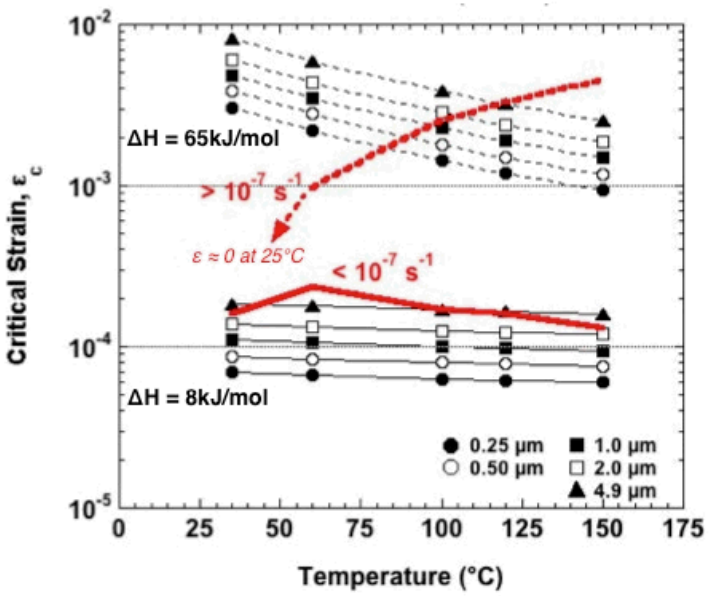

Fig. 10 Graph shows critical strain (ε_c) as a function of temperature and film thickness (different symbols). The benchmark strain rate of 10^{-7} s^{-1} was used in the calculation. The curve sets are designated by ΔH: "ΔH = 65 kJ/mol" curves (dashed lines) and "ΔH = 8 kJ/mol" curves (solid lines). The red curves are the strain contributions at $d\varepsilon/dt > 10^{-7}$ s^{-1} (dashed) and $d\varepsilon/dt < 10^{-7}$ s^{-1} (solid) as predicted by the computational model.

Tables

Film Thickness	Temperature (C)				
	35	60	100	120	150
0.25					
0.5					
1.0					
2.0					
4.9					

Green is present; red is absent.

Table 1 Combination of Long Whisker and Hillock Appearance as a Function of Test Temperature and Film Thickness.